Energy Advances

ROYAL SOCIETY OF CHEMISTRY

PAPER

View Article Online
View Journal | View Issue

Cite this: *Energy Adv.*, 2024, 3, 316

Microwave-assisted valorization of biodiesel byproduct glycerol to solketal over *Musa acuminata* peel waste derived solid acid catalyst: process optimization, kinetics, and thermodynamics†

Rhithuparna Devasan,[ab] Shiva Prasad Gouda,[b] Gopinath Halder [a] and Samuel Lalthazuala Rokhum *[b]

The massive quantity of glycerol produced due to the rapid expansion of biodiesel production requires its transformation into value-added products utilizing novel and sustainable methods. Here we report the microwave-induced production of solketal from glycerol using banana (*Musa acuminata*) peel waste functionalized with sulfonic acid as a heterogeneous catalyst. FTIR, PXRD, TGA, SEM-EDX, and TEM techniques were used to examine the chemical composition and morphology of the catalyst. The four parameters, the glycerol to acetone molar ratio (GTAR), reaction time, catalyst wt.%, and reaction temperature, were optimized using central composite design (CCD). 94.89% glycerol conversion to solketal was observed with a catalyst loading of 7 wt.%, a GTAR of 1 : 4, a reaction temperature of 65 °C, and a reaction time of 12 min. The catalyst showed remarkable stability when used repeatedly and could be reused at least five times without substantial reduction in its activity. With an activation energy of 40.23 kJ mol^{-1}, the reaction followed pseudo-first-order kinetics. The thermodynamic analysis established the endothermic and non-spontaneous nature of the acetalization reaction. Therefore, this technique of glycerol valorization could be applied to the production of solketal as a biofuel additive on an industrial scale with further optimization.

Received 2nd August 2023,
Accepted 3rd December 2023

DOI: 10.1039/d3ya00369h

rsc.li/energy-advances

1. Introduction

Renewable energy exploration will be one of the most important research topics in the next few years due to limited fossil fuel reserves. Due to its excellent flow and combustion properties, biodiesel (fatty acid methyl esters) is considered a cost-effective and highly efficient energy source that can replace fossil fuels completely.[1,2] Compared to regular diesel, it has good lubricating qualities and emits less carbon dioxide.[3,4] The most common method of making biodiesel is through transesterification, which combines triglycerides with alcohols, such as methanol or ethanol, and results in biodiesel as well as crude glycerol as the by-product.[5–8] For every transesterification reaction 10% of glycerol is formed as a byproduct.[9,10]

Several studies have demonstrated that various commercial products can be synthesized from glycerol through different reactions, including acetalization,[11] etherification,[12] and transesterification.[13–15] Specifically, glycerol can be acetalized with acetone to produce solketal (4-hydroxymethyl-2,2-dimethyl-1,3-dioxolane), which is considered to be a value-added product.[16] The liquid solketal is clear and odorless, completely dissolves in water, and is stable under ambient conditions, including temperature and pressure.[17] It is an efficient solvent, anti-freezing agent,[18] and plasticizer.[19] In addition to reducing gum formation and particulate emissions, solketal also increases the octane number and improves the cold flow properties of liquid fuels, making it very popular as a fuel additive that can also reduce emissions.[20,21] Moreover, it is well suited for the polymer industry as well as for pharmaceutical production as a suspension agent.[22,23] An aquatic fish toxicity test found that it was less harmful to the environment than other gasoline additives.[24]

A microwave assisted acetalization reaction for solketal synthesis is a non-contact heat source technique for producing solketal of greater quality with a significantly faster reaction

[a] *Department of Chemical Engineering, National Institute of Technology, Durgapur, West Bengal-713209, India*
[b] *Department of Chemistry, National Institute of Technology, Silchar, Assam-788010, India. E-mail: rokhum@che.nits.ac.in*

† Electronic supplementary information (ESI) available. See DOI: https://doi.org/10.1039/d3ya00369h

rate than conventional heating procedures.[2,14] The desired conversion of glycerol to solketal requires more time using the conventional heating method because the chemical transformation is dependent on the heating efficiency of the reactants, whereas the same conversion is quickly accomplished using uniform and instantaneous heating by microwave irradiation.[25,26] The utilization of a distinctive continuous flow microwave-irradiated reactor equipped with a static mixer, boasting a capacity of 42.5 L h^{-1},[27] facilitates the feasibility of large-scale production at an industrial level. However, implementing microwave technology in industrial environments typically demands a substantial initial investment, possibly creating financial hurdles, especially for smaller businesses. Ensuring the safe operation of microwave equipment requires strict adherence to safety protocols to mitigate risks such as overheating and exposure to high-energy radiation.[28]

The effects of operational parameters such as catalyst wt%, reaction temperature, the glycerol to acetone molar ratio, and time on the acetalization reaction are studied experimentally to optimize the reaction conditions. Manually optimizing one variable at a time (OVAT) consumes a lot of effort, time, and resources. Therefore, response surface methodology-based central composite design (RSM-CCD), a soft computational technique, is used to perform the optimization. RSM-CCD is feasible to more accurately develop a model that can be confirmed using statistical analysis of variance (ANOVA). In addition to demonstrating model accuracy, this technique also determines how interacting variables affect the observed results.[29]

The acetalization of glycerol to solketal has previously been accomplished using a variety of homogeneous and heterogeneous catalysts.[30] Researchers have used a wide range of homogeneous acid catalysts, including HCl, H_3PO_4, divinylbenzene-styrene resin, *p*-toluene sulfonic acid (PTSA), *etc.*, to acetalize glycerol.[31] In comparison to conventional homogeneous catalysts, heterogeneous catalysts offer easy recovery, reduced pollution, and low corrosiveness.[32–34] Solketal synthesis from glycerol has been reported using several solid catalysts, such as metal phosphates,[35,36] metal oxides,[37,38] sulfated carbon,[39–41] resins,[42] clay minerals,[21] sulfated metal–organic frameworks (*e.g.* sulfated UiO-66),[43] mesoporous silica, $Co[II](Co[III]_xAl_{2-x})O_4$,[37] hydrophobic zirconium organophosphonates[36] and zeolites.[44,45] However, they are typically moisture-sensitive, toxic, difficult to prepare, expensive, and unstable. Recently, biomass has garnered great interest as a source of natural catalysts due to its ease of use, benign properties, and economic and environmental benefits.

Solketal production on a large scale is hindered by the cost of catalyst fabrication, despite the potential benefits of carbon-based solid catalysts derived from waste biomass. Hence, a simple, cost-effective, and eco-friendly strategy based on utilizing a waste biogenic heterogeneous catalyst is highly desirable for the production of solketal. According to the report of Statista 2021,[46] the banana market is the world's largest fruit market. It was reported that 124.98 million metric tonnes of bananas were produced in 2021. Furthermore, the cost of disposing banana peels is quite high as they are waste products, and so their beneficial use would boost the economic value of bananas. However, using banana peels as a catalyst source presents a few challenges. Different types of bananas and their degree of ripeness can cause the banana peels to vary in composition, thereby leading to diverse catalytic properties. In addition, the effectiveness of catalysts can also be altered by handling and storage conditions, such as duration, temperature variations, and air exposure. Moreover, the natural breakdown of catalysts may be impacted by the stability of the banana peels over time and the toxicity of components present in them. Despite these challenges, the banana peel is an affordable, readily accessible source of carbon, which can be functionalized with $–SO_3H$ groups by treating it with concentrated H_2SO_4, providing a promising pathway toward the production of solketal.

We have reported the complete synthesis and characterization analysis[13] of an acid-functionalized activated carbon catalyst derived from the banana peel (BP–SO_3H-15-18-100). Thermogravimetric analysis (TGA) of the catalyst showed a major mass loss from 250–500 °C as a result of the decomposition of –COOH, $–SO_3H$, and –OH groups (Fig. S1a, ESI†). Eventually, the powder X-ray diffraction (XRD) study suggested the amorphous structure of the BP–SO_3H-15-18-100 catalyst (Fig. S1b, ESI†). Fourier transform infrared spectroscopy (FTIR) analysis of BP–SO_3H-15-18-100 confirmed the presence of SO_3^- symmetric stretching at 1030 cm^{-1} (Fig. S1c, ESI†). Moreover, the N_2 adsorption–desorption isotherm of the BP–SO_3H-15-18-100 catalyst (Fig. S1d, ESI†) displayed a type IV isotherm with an H3-type hysteresis loop and a surface area, pore volume, and pore diameter of 14.024 m^2 g^{-1}, 0.016 cc g^{-1}, and 2.205 nm, respectively. X-ray photoelectron spectroscopy (XPS) analysis (Fig. S2, ESI†) also showed the presence of C, O, and S, where S in the catalyst is in the form of $–SO_3H$. The scanning electron microscopy (SEM) (Fig. S3a–c, ESI†) and transmission electron microscopy (TEM) analyses (Fig. S3i and j, ESI†) of the catalyst displayed the irregular structure of the catalyst, whereas EDX analysis (Fig. S3g and h, ESI†) results revealed the presence of 4.62 wt% sulfur (S), which corresponds to 1.4437 mmol g^{-1} sulfonic acid density in the BP–SO_3H-15-18-100 catalyst. A thorough examination of many studies that have been published over the past few years shows that, until now, no researchers have used an acid catalyst made from banana peels to produce solketal, particularly under microwave irradiation.

However, the catalyst reported in the present work is used for the acetalization of glycerol with acetone. Since acid-functionalized activated carbons have been shown to be effective as heterogeneous catalysts in a variety of acid-catalyzed reactions,[47] this material is a promising candidate for catalyzing the conversion of glycerol to solketal under green circumstances with high activity and selectivity (solvent-free reaction at mild temperature). Kinetic and thermodynamic studies of the reaction were also performed to determine the rate constant, reaction order, activation energy, and parameters such as enthalpy (*H*), entropy (*S*), and Gibbs free energy (*G*).

2. Experimental methodology

2.1 Materials and methods

Banana peels (*Musa acuminata*) were collected from Aizawl, Mizoram, India. Acetone (98.5%) and glycerol (92.5%) were purchased from Sigma Aldrich. Barium chloride (99.95%), sodium hydroxide (≥97.8%), phenolphthalein (98%), and sulphuric acid (98.07%) were obtained from Merck, India. All chemicals used in this study were of analytical grade, bought from commercial sources, and used as received without further purification.

2.2 Preparation of the catalyst

The banana peels were cut into strips and sun-dried to remove moisture. The dried peels were thoroughly ground into a fine powder and subjected to sulfonation. Through varying the ratios of banana peel powder to sulfuric acid as well as the reaction time and temperature, various banana peel-supported sulfonic acid catalysts (BP–SO_3H) were prepared. The process involved mixing 1 g of banana peel powder rigorously with conc. H_2SO_4 in various ratios of banana peel powder to H_2SO_4 (1 : 5, 1 : 10, 1 : 15, and 1 : 20), with reactions monitored from 16 to 24 h over a temperature range of 80–120 °C in each case. The filtrate was rinsed multiple times using hot deionized water until there were detectable residual sulfate ions left. The presence of sulfate ions was tested using $BaCl_2$ (6 mol L^{-1}) solution (the white precipitate shows the presence of sulfate ions). The resulting sulfonic acid functionalized banana peel (BP–SO_3H) was dried for 24 h in the oven. Each BP–SO_3H catalyst was given a code based on the synthesis parameters: BP–SO_3H–*X*–*Y*–*Z*, where *X* is the weight/volume ratio of banana peel/H_2SO_4, *Y* is the *in situ* hydrothermal sulfonation time, and *Z* is the reaction temperature. As a result, the optimised catalyst BP–SO_3H-15-18-100 was made by utilizing a 1 : 15 (wt/vol) banana peel/sulfuric acid ratio, an 18 h hydrothermal sulfonation period, and a reaction temperature of 100 °C.

2.3 Catalyst characterization

Acid density (–COOH, –OH, and –SO_3H groups) on the surface of the BP–SO_3H catalyst was determined *via* a modified Boehm titration procedure.[48] Basic solutions such as NaOH and $NaHCO_3$ were employed to calculate the overall acid density as well as the combined COOH/–SO_3H density, respectively. 50 mg of the catalyst was dissolved in 15 mL of 2 M NaCl solution and thoroughly stirred for 24 h. The filtered reaction mixture was titrated using a phenolphthalein indicator against a 0.02 M NaOH solution. Between 50 and 600 °C, thermogravimetric analysis (TGA) was performed using a PerkinElmer instrument (TGA 4000) under continuous flow of N_2. On an X'Pert Pro (PANalytical, Holland) diffractometer, powder X-ray diffraction (XRD) patterns were obtained using a tube current of 100 mA and a generator voltage of 40 kV. XRD was performed using Cu Kα radiation with 2θ = 10–60°. Using a Micromeritics ASAP 2010 (USA) surface area and porosity detector, the sample was degassed for 10 hours at 150 °C, which was analyzed using the Brunauer–Emmett–Teller (BET) technique. Fourier transform infrared spectra (FTIR) were recorded on KBr pellets using a Nicolet 6700 (Nicolet Instrument Co., USA) spectrophotometer. Scanning electron microscopy (SEM) and energy-dispersive X-ray spectroscopy (EDX) were performed using a JEOL JSM-7600F (Japan) microscope at a magnification of 1500×, 20 kV laser voltage, and 80 mA beam current. After being dispersed in ethanol, the catalyst was dropped on a Cu grid drop-by-drop before it was oven dried. High-resolution transmission electron microscopy (HRTEM) was performed using an electron microscope from JEOL (Japan), JEM-2100, at 200 kV. X-ray photoelectron spectroscopy (XPS) analysis was conducted using a Thermo Fisher Scientific's ESCALAB Xi+ device (USA).

2.4 Acetalization of glycerol to solketal on a laboratory scale

The developed catalyst was used for the microwave-induced acetalization of glycerol (Scheme 1). The catalyst was mixed thoroughly with glycerol and acetone in a microwave tube. The first stage of the reaction involves the activation of acetone by the acid sites of BP–SO_3H-15-18-100, resulting in intermediate **1**, which then undergoes cyclization to produce 2,2-dimethyl-1,3-dioxolan-4-yl methanol (solketal) (**2**) and/or 6-membered cyclic 2,2-dimethyl-1,3-dioxan-5-ol (**3**). The formation of **3** is not kinetically favourable, so the reaction normally prefers **2**.[49] In the present work, a selectivity of 97.53% was achieved for compound **2** over **3** in the initial catalytic cycle, with water being produced as a by-product. For finding optimal reaction conditions, the glycerol to acetone molar ratio (GTAR), catalyst weight percent, reaction time, and temperature were varied in batch studies keeping one factor constant at a time (OFAT). The obtained data were fed in RSM-CCD to design an experimental matrix with distinct combinations of parameters for each run. The optimized reaction conditions were glycerol (1 mmol) and acetone (4 mmol) in a 1 : 4 molar ratio and 7 wt% catalyst at 65 °C for 12 min. The progression of the reaction and the production of solketal were observed using thin-layer chromatography (TLC). TLC results indicated complete conversion, leading to the isolation of the freshly synthesized solketal. A rotary evaporator was used to concentrate the filtered solution to remove excess acetone. Following the reaction, the catalyst was recycled, and its catalytic activity was tested five more times.

Solketal was subjected to GC-MS and NMR analysis to confirm its formation. GC-MS analysis was executed using an Agilent (6890) gas chromatography instrument linked with an Agilent 5973 mass spectrometer (Agilent Technologies, USA). NMR analysis was carried out using an AVANCE III 500 MHz NMR spectrometer (USA). Furthermore, eqn (1) and (2) were used to evaluate the conversion of glycerol to solketal and the selectivity of solketal respectively.

$$\text{Glycerol conversion}\,(\%) = \frac{M_{GC}}{M_G'} \times 100 \quad (1)$$

$$\text{Solketal selectivity}\,(\%) = \frac{M_{SF}}{M_{GC}} \times 100 \quad (2)$$

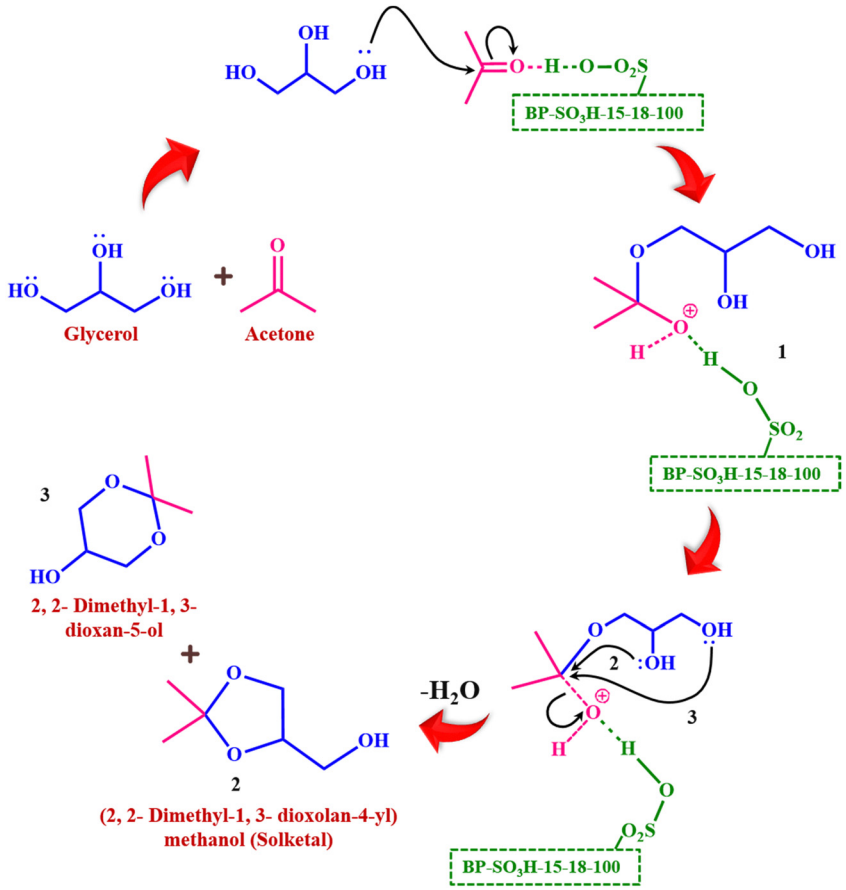

Scheme 1 Proposed mechanism of glycerol acetalization using the BP–SO_3H-15-18-100 catalyst.

where M_{GC} = the mole of glycerol converted, $M_G^{'}$ = the initial mole of glycerol, and M_{SF} = the mole of solketal formed.

2.5 Experimental design for optimization by means of the RSM-CCD matrix

This study examined 30 experimental runs of three-level, four-factor central composite design (CCD). Stat-Ease Inc.'s Design Expert version 13.0 software from Minneapolis, Minnesota, USA, was utilized for the model's regression analysis. The design levels and ranges of reaction parameters are presented in Table 1. Conversion % of glycerol to solketal was used to assess the effects of various factors and the efficiency of the optimization process. The performance and interaction of the components in glycerol conversion are calculated using a quadratic polynomial equation, as shown in eqn (3)

$$\text{Glycerol conversion } (Y) = x_0 + x_1A + x_2B + x_3C + x_4D + x_{12}AB + x_{13}AC + x_{14}AD + x_{23}BC + x_{24}BD + x_{34}CD + x_{11}A^2 + x_{22}B^2 + x_{33}C^2 + x_{44}D^2 \quad (3)$$

where A, B, C, and D are the coded factors (A = glycerol to acetone molar ratio, B = catalyst loading, C = reaction time, and D = temperature), x_0 = intercept term, x_{1-4} = coefficients of linear terms, x_{12-14}, x_{23}, x_{24}, x_{34} = coefficients of interaction terms, and x_{11}, x_{22}, x_{33}, x_{44} = coefficients of quadratic terms. An equation for quadratic regression that revealed the maximum possible glycerol conversion verified the accuracy of the experimental results. Both the model and the sum of squares of the individual factors were used as shown in eqn (4), to investigate the effect of the final glycerol conversion and the extent to which each parameter contributed.

$$\text{Contribution factor } (\%) = \left(\frac{SS_f}{SS_T}\right) \times 100 \quad (4)$$

where SS_T = sum of squares of the model and SS_f = sum of squares of a particular factor.

Table 1 Values of process parameters at different levels

	Name	Units	Low	High	−Alpha	+Alpha
A	GTAR	Molar ratio	3	5	2	6
B	CL	wt%	5	9	3	11
C	Time	min	10	14	8	16
D	Temp	°C	55	75	45	85

3. Results and discussion

3.1 Characterization of solketal

The catalyst was successfully prepared and characterized before being employed to acetalize glycerol with acetone to generate solketal. Mixing glycerol with acetone was carried out in a molar ratio of 1 : 4. This was followed by adding 7 wt% of the catalyst with respect to glycerol. For the best glycerol conversion of 94.89%, the reaction was agitated in a microwave reactor at 65 °C for 12 min. The mixture was filtered using Whatman 41 filter paper to isolate the catalyst. Alumina sheet TLC (02665) was used to evaluate the conversion of glycerol to solketal. It was then rinsed with ethanol and concentrated using a rotary evaporator to eliminate excess ethanol. The produced solketal was subjected to NMR and GC-MS analysis. Spectroscopic measurements of ^{1}H and ^{13}C NMR (Fig. S4, ESI†) confirmed that the product was 2,2-dimethyl-1,3-dioxolane-4-methanol. ^{1}H NMR (500 MHz, $CDCl_3$) δ ppm: 4.12 (m, 1H, CH), 3.94 (dd, 2H, CH_2), 3.68 (dd, 2H, CH_2), 1.33(s, 3H, Me) 1.26 (s, 3H, Me). ^{13}C NMR (126 MHz, $CDCl_3$) δ ppm: 109.36 (MeCMe), 76.27 (CH_2CHCH_2), 65.88 (OCH_2CH), 62.86 (CH_2OH), 26.68 (Me), 25.26 (Me). Two different singlets represent the six-methyl hydrogen of 1,3-dioxolane in the ^{1}H NMR spectrum (Fig. S4a, ESI†) of the glycerol acetalization product at 1.33 and 1.26 ppm. The –CH and –CH_2 groups present in the product structure are represented by peaks at 4.15–3.66 ppm. Fig. S4b (ESI†) depicts the ^{13}C NMR spectrum of solketal. The most protected peaks, which appear at 25.26 and 26.68 ppm, are attributed to methyl carbons. The peak at 76.27 ppm is attributed to the –CH carbon, while the peaks of the two –CH_2 carbons are observed at 65.88 and 62.86 ppm. The peak at 109.36 ppm, which is the most deshielded peak, is attributed to the ketal carbon. These two spectra unequivocally demonstrate that a 5-membered solketal product is generated during glycerol acetalization.[50]

In the GC-MS study (Fig. S5, ESI†), two sharp peaks at 4.058 min and 4.490 min, respectively, indicated the production of the *R* and *S* isomers of solketal. This offers additional evidence that solketal was synthesized precisely and specifically. A tiny amount of glycerol was retained, as evidenced by the peak at 4.433 min. Between the peaks of solketal and glycerol, no peaks were observed. As a result, the six-membered ring (acetal) did not form, demonstrating the acetalization of glycerol's complete selectivity for synthesizing solketal.

3.2 Modelling and analysis of data using response surface methodology (RSM)

A central composite design (CCD) experimental matrix of RSM was used to optimize the acetalization reaction. Based on the laboratory tests, actual glycerol conversion ranged from 55.05 to 94.89 wt%. The outcomes of the acetalization reactions examined using a microwave-assisted method are shown in Table 2. Meanwhile, the following equation describes how the conversion is related to the coded factors in response to independent variables:

Table 2 CCD experimental design matrix for acetalization of glycerol to solketal

Run	Space type	GTAR molar ratio (*A*)	Catalyst loading wt% (*B*)	Time min (*C*)	Temp °C (*D*)	Actual solketal conversion (%)	Predicted solketal conversion (%)
1	Factorial	3	5	14	55	76.05	76.08
2	Center	4	7	12	65	94.89	94.32
3	Center	4	7	12	65	94.02	94.32
4	Center	4	7	12	65	94.65	94.32
5	Factorial	5	5	14	55	80.45	80.70
6	Factorial	3	5	14	75	71.01	70.60
7	Factorial	3	9	10	55	70.2	70.55
8	Factorial	5	5	10	75	78.5	79.17
9	Axial	4	7	12	45	90.91	90.65
10	Axial	4	7	12	85	84.02	83.42
11	Factorial	3	5	10	55	86.84	87.25
12	Axial	4	3	12	65	63.28	63.14
13	Factorial	3	5	10	75	86.75	86.83
14	Center	4	7	12	65	94.2	94.32
15	Axial	4	7	16	65	81.51	81.38
16	Axial	4	11	12	65	55.05	54.33
17	Center	4	7	12	65	94.09	94.32
18	Axial	6	7	12	65	84.34	83.46
19	Factorial	5	9	10	55	65.89	66.41
20	Factorial	3	9	14	75	76.1	77.14
21	Factorial	3	9	10	75	71.11	70.97
22	Factorial	5	5	10	55	82.05	81.76
23	Factorial	5	9	14	75	81.24	80.94
24	Axial	2	7	12	65	85.12	85.15
25	Factorial	5	5	14	75	72.65	73.05
26	Factorial	5	9	14	55	87.08	87.75
27	Factorial	5	9	10	75	63.96	64.67
28	Axial	4	7	8	65	77.01	76.28
29	Factorial	3	9	14	55	82.34	81.78
30	Center	4	7	12	65	94.05	94.32

$$\text{Glycerol conversion } (Y)\ \% = 94.32 - 0.4225A - 2.20B + 1.28C - 1.81D + 0.3388AB + 2.53AC - 0.5412AD + 5.60BC + 0.2113BD - 1.27CD - 2.50A^2 - 8.89B^2 - 3.87C^2 - 1.82D^2$$

where A, B, C, and D are the coded factors (A = glycerol to acetone molar ratio, B = catalyst loading, C = reaction time, and D = temperature). The "+" and "−" symbols in the regression equation denote whether a certain term has a positive or negative impact on the response process and correspond to a particular level of the process parameter. Based on their contribution factors, the significant parameters are glycerol to acetone concentration = 0.13%, catalyst loading = 3.56%, reaction temperature = 2.39%, and time = 1.19%.

Analyzing and interpreting experimental results were executed using statistical analysis of variance (ANOVA). Table 3 contains the results of the statistical evaluation of the entire procedure. In ANOVA, the Fischer test (F-value) was used to determine the parameter impacts and significance of the model structure. A parameter or model with a higher F-value holds more significance in the process. The present study's quadratic model had an F-value of 506.80, clearly showing its significance. The F-value was also attributed to be less likely than 0.01% to be caused by noise. The probability that an F-value will exist regardless of the size is represented by the p-value, where $p < 0.05$ implies the significant terms in the model.[51] The experimental data fit perfectly to the chosen model according to the obtained correlation coefficient R^2, 0.9979. It was determined that the model was suitable for navigating the design space, with an adequate precession of 83.44, above 4 being considered desirable because it also measures the signal-to-noise ratio. The model had a C.V.% of 0.840, which indicates a reasonable correlation between predicted and actual conversion, where a value of at least 10% is desirable.

Diagnostic plots (Fig. 1) are employed to gauge the effectiveness of the regression model. An illustration of the relationship between normal distribution and studentized residuals can be seen in Fig. 1a. The graph demonstrates that the majority of datasets are linear, as opposed to the unique S-shaped distribution that characterizes a normal distribution. The relationship between the predicted glycerol conversion and the studentized residuals is shown in Fig. 1b. The random distribution of residuals in the plot shows that there is no relationship between the response values and initial observations. Thus, no transformation of the response parameter is necessary. In Fig. 1c, the residuals are compared with the results of the experimental run. Large residual variations across runs are seen, considering the noise that the trials introduced. Particular trends or patterns were not evident in independent residuals. The random distribution of residuals around the central axis of the plot made the fitted model fall within the range of 4.00, because of which no errors were recorded. A comparison between the predicted and actual glycerol conversion is shown in Fig. 1d. All responses had close correlations between actual and predicted values. Based on these findings, the model is suitable for predicting maximum glycerol conversion using empirical data.

3.3 Parametric analysis of conversion

3D surface model plots were employed to assess the impact of the four independent variables (catalyst loading (CL), temperature, time, and GTAR) on glycerol conversion as shown in Fig. 2. As other parameters remain constant at their center values, it is possible to observe the interaction of two variables on the model graphs. With the increase in time from 10 to 14 min, the glycerol conversion also increased, and the surface graphs demonstrated that the conversion rose until it reached its maximum at 12 min, after which it decreased despite an increase in catalyst loading, GTAR, and temperature. Similarly, the influence of temperature (60–80 °C), catalyst loading (5–9 wt%), and the glycerol to acetone molar ratio (1 : 3–1 : 5) on the glycerol conversion was also examined.

Table 3 Statistical ANOVA results for acetalization of glycerol to solketal

Source	Sum of squares	df	Mean square	F-Value	p-Value		Accuracy test	
							Parameters	Values
Model	3257.85	14	232.70	506.80	<0.0001	Significant	R^2	0.9979
A-GTAR	4.28	1	4.28	9.33	0.0080		Adjusted R^2	0.9959
B-CL	116.34	1	116.34	253.37	<0.0001		Predicted R^2	0.9887
C-Time	39.07	1	39.07	85.08	<0.0001		Adequate precision	83.4453
D-Temp	78.34	1	78.34	170.61	<0.0001		Std. Dev.	0.6776
AB	1.84	1	1.84	4.00	0.0640		Mean	80.65
AC	102.11	1	102.11	222.39	<0.0001		C.V.%	0.8402
AD	4.69	1	4.69	10.21	0.0060			
BC	501.54	1	501.54	1092.29	<0.0001			
BD	0.7140	1	0.7140	1.56	0.2315			
CD	25.65	1	25.65	55.87	<0.0001			
A^2	171.91	1	171.91	374.41	<0.0001			
B^2	2170.08	1	2170.08	4726.16	<0.0001			
C^2	411.02	1	411.02	895.14	<0.0001			
D^2	90.83	1	90.83	197.82	<0.0001			
Residual	6.89	15	0.4592					
Lack of fit	6.22	10	0.6223	4.69	0.0510	Not significant		
Pure error	0.6639	5	0.1328					
Cor total	3264.74	29						

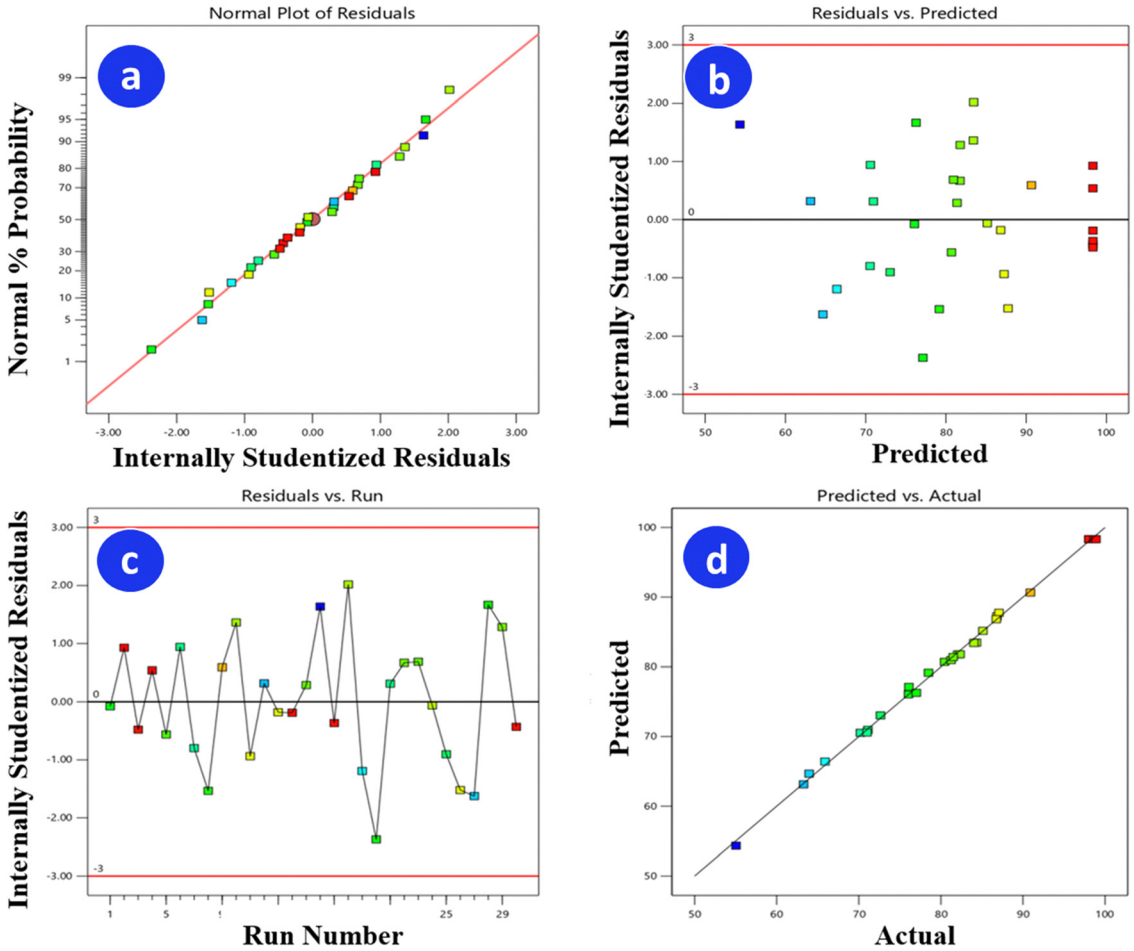

Fig. 1 Diagnostic plots of (a) normal regression plot, (b) studentized residuals *vs.* predicted glycerol conversion, (c) residual differences between predicted and actual conversion of experimental runs, and (d) predicted % glycerol conversion *versus* actual % glycerol conversion.

The interactive effect of the GTAR with parameters like catalyst concentration and time (Fig. 2a and b) demonstrates a linear relationship, and the glycerol conversion is observed to decline after the central point of the maximum is attained. Variations in temperature throughout the range of 55 to 75 °C were examined in the conversion of glycerol. Fig. 2c shows the combined effect of reaction temperature and the glycerol to acetone molar ratio on glycerol conversion over a 12 min reaction time with a catalyst loading of 7 wt%. An increase in reaction temperature and the GTAR increased the solketal concentration, and the study showed that optimal conditions for temperature and the GTAR resulted in the highest conversion of glycerol. Nevertheless, the glycerol conversion increased until the specified reaction temperature and GTAR value. Higher GTAR values result in lower glycerol conversion, which makes product separation more challenging. Similarly, production also decreased with the increase in temperature above 65 °C. Despite using a pressure environment, acetone still evaporates, resulting in decreased conversion.[30] As solketal is a kinetically controlled product, increasing the temperature may facilitate a more rapid formation of the thermodynamic product (six-membered ring).[52] As a result, the highest glycerol conversion was observed at a 1 : 4 GTAR at 65 °C.

The rate of acetalization of crude glycerol in response to the combined effects of catalyst concentration and the reaction temperature is shown in Fig. 2e, maintaining the constant value of GTAR (1 : 4) and reaction duration (12 min). In contrast, Fig. 2d illustrates how the catalyst amount and reaction time affect glycerol conversion. With the prescribed amount of catalyst, a gradual rise in reaction temperature impacted the rate of glycerol acetalization. Increasing the catalyst concentration from 5–7 wt% led to the improved synthesis of solketal due to the more active sites available on the catalyst. Hydrolysis of the product caused by increasing the catalyst concentration to 9 wt% lowered the product formation.[53]

The combined effect of temperature and time on glycerol conversion is depicted in Fig. 2f. Glycerol conversion increased significantly as the reaction temperature and time were linearly related. An increase in the conversion up to 12 min might be because of the increase in the number of reacting molecules causing the formation of new bonds after cleaving the preexisting bonds.[52] As time progressed, the product may have hydrolyzed by forming water, explaining the drop in conversion.[53]

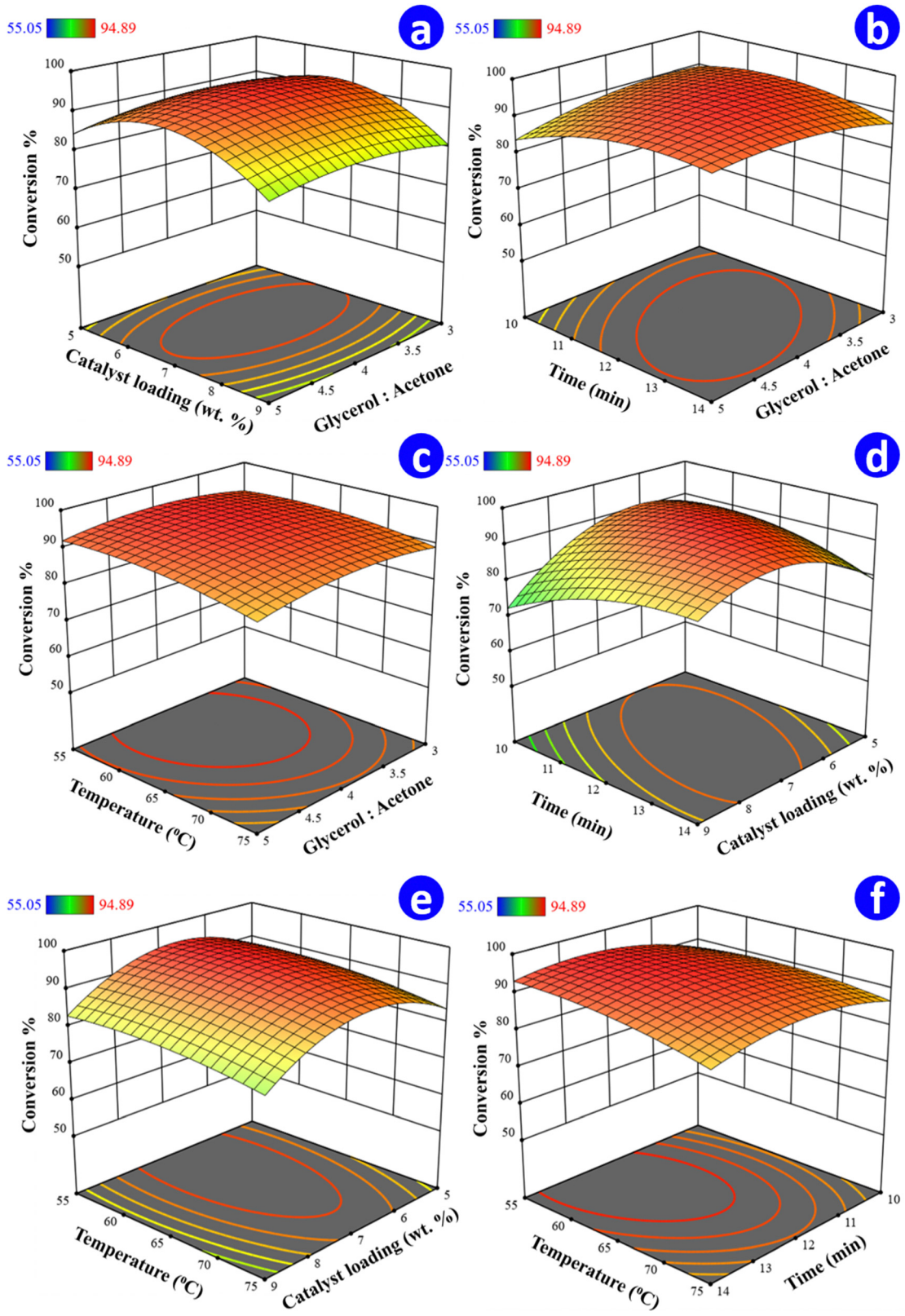

Fig. 2 3D surface plot depicting the interaction of the independent variables *A*–*D* and their effect on the efficiency of microwave-assisted solketal synthesis from glycerol.

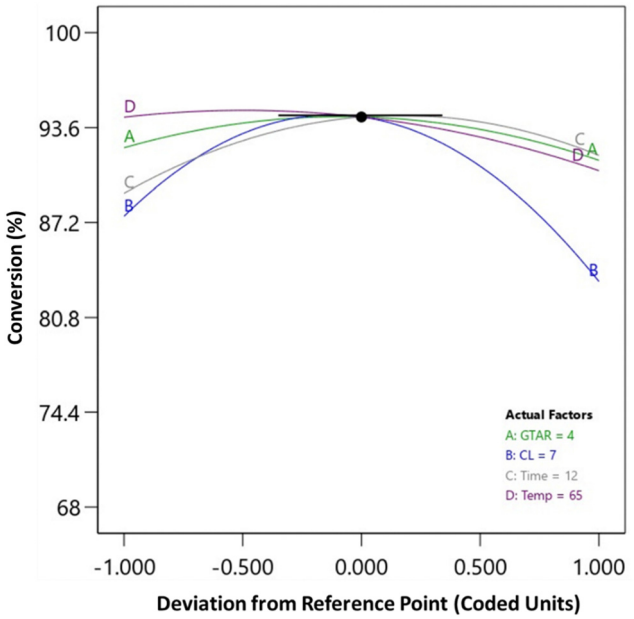

Fig. 3 Perturbation plot exhibiting significant variables affecting glycerol conversion.

Therefore, for the 12 min optimal reaction time, a reaction temperature of 65 °C was more favorable.

In order to classify the impact of the process variables on conversion while maintaining the other process variables at an intermediate level, the perturbation plot (Fig. 3) was used. The curvature characteristics are a representation of the variability of *A* to *D* factors in the glycerol conversion. Glycerol conversion is more significantly impacted by a factor with a steeper slope than the one with a flatter slope. Thus, from Fig. 3, it is the factor *B* that displays the highest impact on glycerol conversion, followed by factors *D*, *C*, and *A*. This also demonstrates that the sensitivity of the catalyst loading (*B*) increases from the medium level to the higher level but decreases between the intermediate and lower levels. *D* and *C* have a significant impact on conversion between intermediate and higher level parameters. In comparison to the higher-intermediate range, the variation in glycerol conversion below the intermediate level is moderate.

3.4 Optimization of glycerol conversion to solketal

The optimal set of conditions for the four input variables, with a desirability function of 1, were discovered using a numerical optimization approach. This strategy aimed to maximize glycerol conversion within the lower and upper limits of the study's variables. The RSM-CCD technique gave the ideal conditions for the acetalization of glycerol: a reaction temperature of 58.81 °C, a reaction duration of 12.66 min, a GTAR of 4.2, and a catalyst loading of 6.85 wt.% under microwave irradiation, with a glycerol conversion of 95.00 wt.%. Furthermore, a conversion of 94.89% was obtained during laboratory tests carried out under the RSM optimised conditions, showing that the regression model proposed is beneficial for comprehending the acetalization process.

4. Kinetics and thermodynamics study

Given the excess acetone in the reaction, it was anticipated that the acetalization process would follow pseudo-first-order kinetics, negating the reverse reaction.[54] As a result, the rate of the reaction (r_S) of solketal formation can be expressed as follows:

$$r_S = k[G] = -\frac{d[G]}{dt} \quad (5)$$

where [G] = glycerol concentration, k = reaction rate constant, and t = reaction time. Calculating the rate constant of the reaction required altering the time and monitoring the conversion of glycerol following eqn (6). Using the rate constant values by varying the temperature from 50 to 65 °C, the Arrhenius equation (eqn (7)) was used to calculate the activation energy (E_a).

$$-\ln(1 - X) = kt \quad (6)$$

$$\ln k = -\frac{E_a}{RT} + \ln A \quad (7)$$

Here, R is the universal gas constant (8.314 J K^{-1} mol^{-1}), X indicates the amount of glycerol converted at time t, A and T represent the pre-exponential factor and the reaction temperature, respectively.

Additionally, to understand how temperature affects the conversion of glycerol, a thermodynamic analysis of the acetalization reaction was also carried out. It is crucial to consider thermodynamic parameters such as enthalpy (H°), Gibbs free energy (G°), and entropy (S°) when assessing whether a reaction is spontaneous or not. Eqn (8) illustrates how thermodynamic parameters are related according to the Eyring–Polanyi relationship. Likewise, Gibbs's free energy can be calculated using H° and S° through eqn (9).

$$\ln\frac{k}{T} = \frac{\Delta S^\circ}{R} - \frac{\Delta H^\circ}{RT} + \ln\left(\frac{k_b}{h}\right) \quad (8)$$

$$\Delta G^\circ = \Delta H^\circ - T\Delta S^\circ \quad (9)$$

Here, h = Planck's constant (6.626×10^{-34} J s) and k_b = Boltzmann constant (1.38065×10^{-23} J K^{-1}).

For reactions occurring between 50 and 65 °C, $-\ln(1 - X)$ shows a linear relationship with time (Fig. 4a), supporting our hypothesis that acetalization follows pseudo-first-order kinetics.[2] The activation energy (E_a) of the acetalization reaction was determined by substituting rate constants in the Arrhenius equation (eqn (7)). A pseudo-first-order kinetic model is developed using a plot of $\ln k$ *versus* T^{-1}, as shown in Fig. 4b. The values of E_a and pre-exponential factor (A) are determined by equating the slope and intercept from the graph. Based on Fig. 4b, a pre-exponential factor of 5.9×10^5 min^{-1} and an E_a of 40.23 kJ mol^{-1} were calculated. As shown in Table 4, ΔH° and ΔS° are determined by computing the slope and intercept of Fig. 4c. Entropy and enthalpy changes were found to be −140.3 J K^{-1} mol^{-1} and 38.56 kJ mol^{-1},

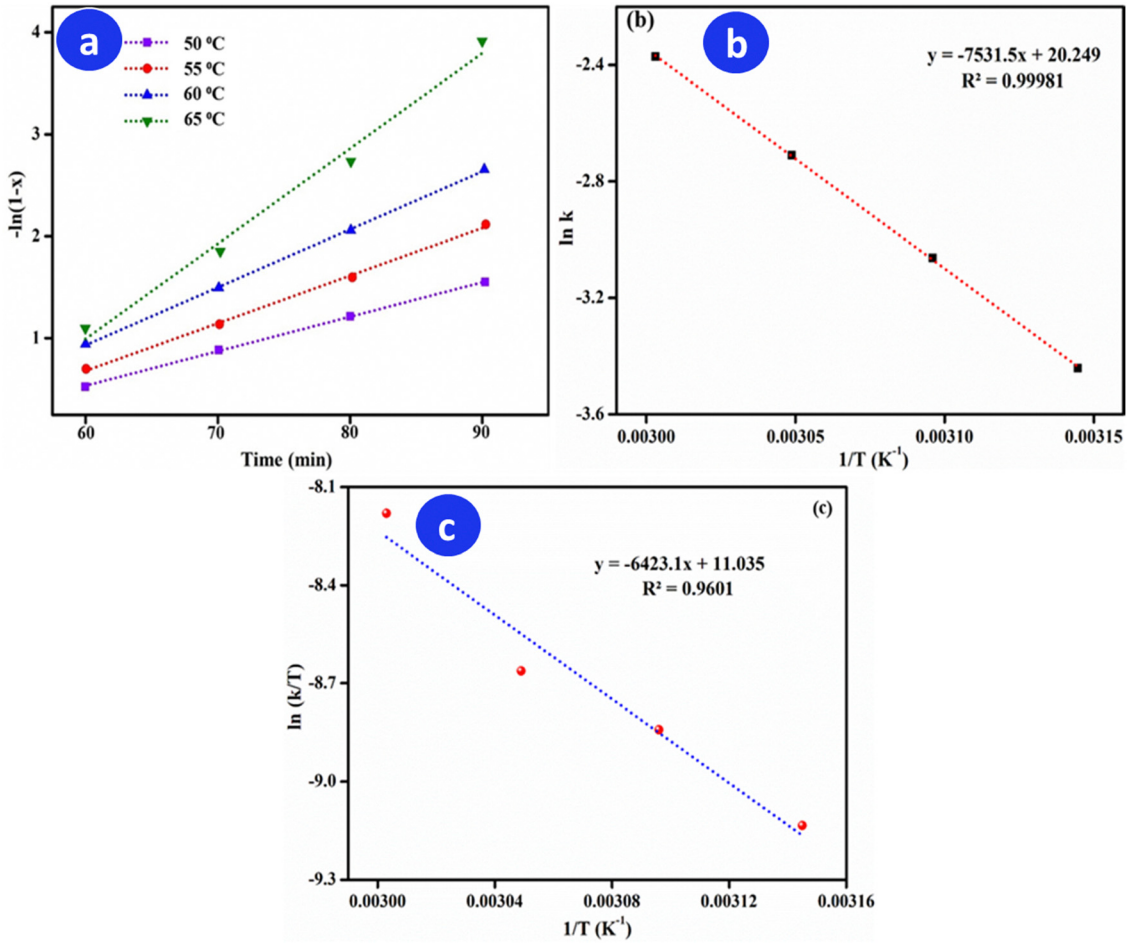

Fig. 4 (a) Plot of $-\ln(1 - X)$ *vs.* time, where X = glycerol conversion at different temperatures for acetalization reaction, (b) the corresponding Arrhenius plot of $\ln k$ *vs.* $1/T$, and (c) thermodynamic behaviour of acetalization reaction.

Table 4 Thermodynamic parameters for solketal production from glycerol using the BP–SO_3H-15-18-100 catalyst

Temperature (K)	ΔG° (kJ mol^{-1})	ΔH° (kJ mol^{-1})	ΔS° (J K^{-1} mol^{-1})
323	83.87		
328	84.57	38.56	−140.3
333	85.27		
338	85.98		

respectively. The values of ΔH° and ΔS° were substituted in eqn (9) to obtain the value of ΔG° for temperatures ranging from 323–338 K. The reaction is proven to be less disordered and endothermic due to the negative value of ΔS° and the positive value of ΔH°. The reaction is non-spontaneous, as evidenced by the positive values of ΔG° (refer Table 4).

5. Reusability of the catalyst

A vital characteristic of a solid heterogeneous catalyst is its ability to be reused. The reusability of the catalyst was tested by acetalizing glycerol using recycled catalysts under optimized conditions (GTAR – 1 : 4, catalyst loading – 7 wt%, reaction time – 12 min, and reaction temperature – 65 °C). After each catalytic run, the recovered catalyst was filtered to remove physisorbed compounds, followed by washing with chloroform and methanol. Prior to use in the subsequent cycles, the catalyst was placed in an oven and dried overnight at 80 °C. It was observed that glycerol conversion decreased mildly with repeated catalyst recycling. Outstanding catalytic activity was observed along with a five-time reusability limit with no discernible activity loss. Every subsequent cycle displayed a decrease in glycerol conversion until it reached 83.48% in the fifth cycle (Fig. 5a). This slow and constant deactivation is due to surface poisoning by unreacted glycerol,[55] as evident from ^{13}C ssNMR data (shown in Fig. S6, ESI†) after 5 cycles displaying remnant glycerol in the catalyst matrix at 55–75 ppm, which is absent in the fresh catalyst and possibly could be attributed to the interaction of –CO_2H and –SO_3H acid sites with the remnant glycerol, leading to the formation of carboxylate and sulfonate esters.[56,57] After the fifth reuse, SEM analysis showed that fresh and recovered catalysts had similar morphologies. According to EDX (Fig. 5b and c) analysis of the 5th recycled catalyst, S content decreased from 4.62 wt% to 3.9 wt%, indicating that repeated reuse might result in decreased catalytic activity.

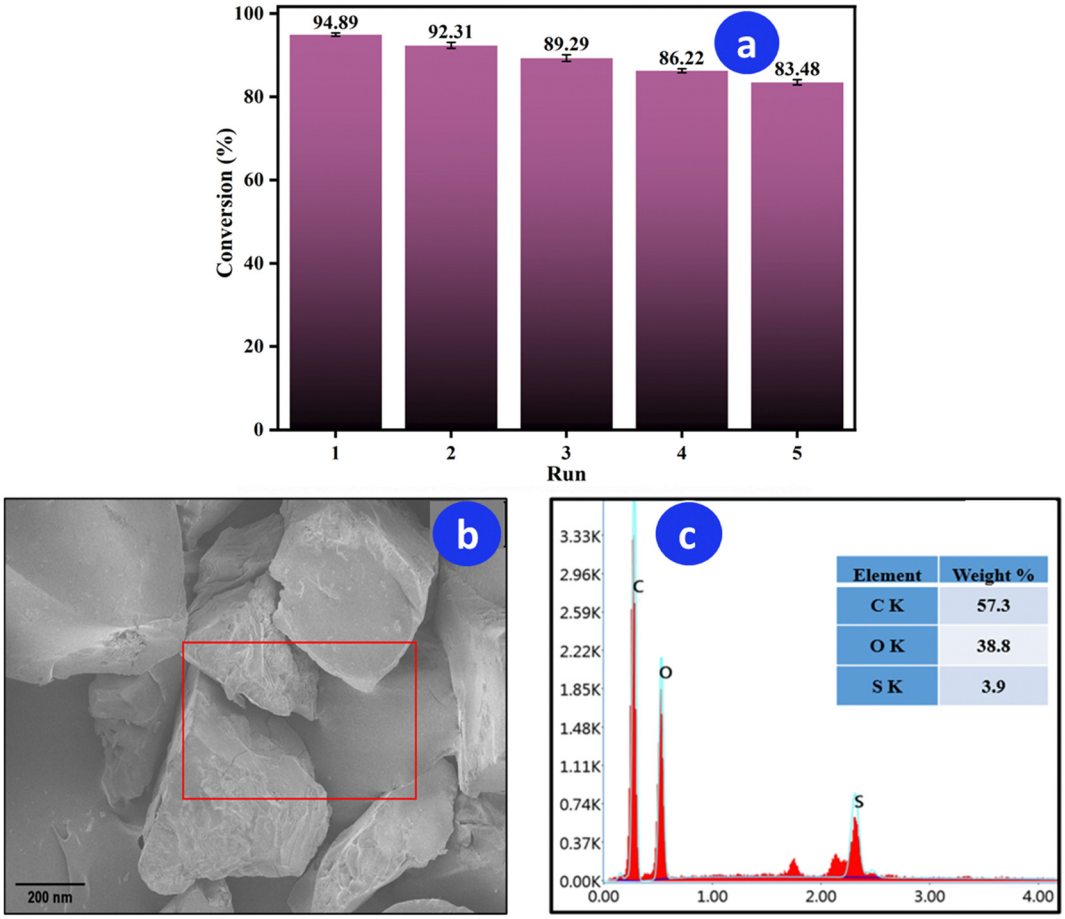

Fig. 5 (a) Graphical representation of reusability of the catalyst over 5 cycles for acetalizing glycerol and (b) SEM and (c) EDS spectra of the recovered catalyst.

6. Comparison with the previously reported catalysts

As shown in Table 5, various catalysts published in the literature were compared to the present catalyst in acetalization reactions. It has been found that most of these convert glycerol to solketal efficiently. However, there are several drawbacks, including a high GTAR (entries 3 and 10), long reaction times (entries 3, 4, 7, 9, 10, 11, and 12), high temperature (entries 4, 8, and 9), and high catalyst loading (entries 1 and 10). One of the parameters used to assess a catalyst's efficiency is its turnover frequency (TOF) (eqn (S1), ESI†). TOF has gained popularity

Table 5 Comparison of the present catalyst with previously reported catalysts

Entry	Catalyst used	GTAR	Catalyst loading (wt%)	Reaction temperature (°C)	Reaction time (min)	Selectivity (%)	Glycerol conversion (%)	TOF (mol g^{-1} h^{-1})	Ref.
1.	Amberlyst 15	1 : 5	10	60	30	32	88.00	0.1910	58
2.	Sulphated zirconium oxide	1 : 6	0.6	40	60	88	80.00	1.449	59
3.	Ni–Zr supported on mesoporous activated carbon	1 : 8	4	45	180	74	100.00	0.0905	52
4.	Hf-TUD-1	1 : 1	3	80	360	100	65.00	0.0392	55
5.	Amberlyst Wet	1 : 6	6.25	40	15	97	88.00	0.6127	21
6.	PSF/K–SiO_2	1 : 10	5	25	90	97.7	86.30	0.1250	60
7.	Arenesulfonic acid-functionalized silica	1 : 6	5	70	30	81	84.00	0.3652	61
8.	Zr–TUD-1	1 : 1	3	80	360	100	64.00	0.0386	55
9.	WO_X/MCM-41	1 : 6	10	50	120	—	78.52	0.0426	62
10.	$(C_3H_7)_4/N^+$PWA (K10 clays)	1 : 6	3	30	120	98	94.00	0.1702	17
11.	Acid-functionalized activated carbon	1 : 4	2.7	28	360	> 93	97.00	0.0650	63
12.	BP–SO_3H-15-18-100	1 : 4	7	65	12	97.53	94.89	0.7303	Present work

Table 6 Stepwise catalyst preparation costs

Approximate cost estimation for 1 kg catalyst production		
Step	Description	Amount
Cost of starting material (CSM)	Waste biomass is collected from local areas of Mizoram. 10% extra cost accounted for industrial scale production.	0
Cost of size reduction (CSR)	Manual reduction. 10% extra costs are allocated to machine reduction.	$0
Cost of drying raw material (CDR)	Time in hour × consumed unit × cost/unit = 10 × 1 × $0.061	$0.61
Total cost of raw material (CRM):	CSM + CSR + CDR = $0 + $0 + $0.061	$0.061
Impregnation cost (IC) = CHC (chemicals cost) + RC (rotation costs)	CHC = [H_2SO_4 quantity needed (L) × cost/L] = 8 × $7.09 = $56.72	
RC = time (hour) × consumed unit × cost/unit = (0.5 × 1 × $0.061) = $0.030	IC = $56.72 + $0.03	$56.75
Carbonization cost (CC) = EH (expense of heating) + IAC (inert atmosphere costs)	EH = time (hour) × consumed unit × cost/unit = 18 × 6 × $0.061 = $6.588	
	IAC = flow of N_2 = $0.041	
	CC = $6.588 + $0.041 = $6.629	$6.629
Washing cost (WC)	WC = units consumed × unit cost for 1 L water = 1 × $0.061	$0.061
Drying cost (DC)	DC = time in hour × consumed unit × cost/unit = 24 × 1 × $0.061	$1.464
Net cost	CRM + CI + CC + WC + DC = $0.061 + $56.75 + $6.62 + $0.061 + $1.464	$64.95
Cost of catalyst (kg)	= net cost + overhead costs (10% of extra cost) = $64.95 + $6.495	$71.45
Cost of total (1 kg) catalyst	= cost of one-time use/no. of use in reusability = $71.45/5	$14.29

Table 7 Cost associated with 100 kg solketal production

Step	Description	Cost
Cost of glycerol to produce 100 kg solketal	Amount (kg) × glycerol cost per kg = 75.3 kg × $0.84 = 63.25	$63.25
Cost of catalyst to produce 100 kg of solketal	Amount (kg) × catalyst cost per kg = 5.2 × $14.29	$74.30
Cost of acetone required to produce 100 kg of solketal	After 5 cycles, the acetone cost for production of 100 kg of solketal = (amount (kg) × acetone cost per kg) − 5 = (189.95 × $0.48) − 5 = $18.23	$18.23
Production cost of solketal ((acetalization time (h) × units × per unit cost))	= 0.2 h × 6 × $0.061 = 0.0732	$0.0732
Extra charges (cost of washing + multifarious)	$1.80	$1.80
Cost of solketal (100 kg)	$63.25 + $74.30 + $18.23 + $0.0732 + $1.80	$157.65
Overhead cost (10% of net cost)	$1.57	$1.57
Solketal cost (100 kg)	$157.65 + $1.57 = $159.22	$159.22
Solketal cost (1 kg)	$1.59	$1.59

among industrial researchers, particularly when it comes to quantifying catalyst activity. Most of the reported catalysts had a turnover frequency less than that of BP–SO_3H-15-18-100, which was 0.7303 mol g^{-1} h^{-1}, however, sulphated zirconium oxide had a higher TOF value at the expense of lower conversion and selectivity than the present catalyst.

7. Cost analysis of catalyst preparation and solketal production

The viability of economically scaling up the acetalization process for the large-scale production of solketal is greatly influenced by the catalyst's cost-effectiveness and performance. Hence, it is extremely important to judiciously select waste precursor materials that are readily available in nature for the preparation of catalysts to reap the benefits they can offer. The expenses associated with the catalyst preparation and solketal production help in assessing the applicability of the method in real-world scenarios taking into account all the factors such as raw material sources, production methods, treatment processes, and reusability of spent catalysts. Table 6 displays an overview of the catalyst's cost analysis, calculated in US dollars ($). The estimated cost of 1 kg of BP–SO_3H-15-18-100 was calculated to be $14.29. This considerable cost reduction is attributable to the reusability of the catalyst. Table 7 summarizes the stepwise cost of solketal production.

8. Conclusion

This study aimed to synthesize and apply the sulfonic acid doped banana peel (BP–SO_3H-15-18-100) as a heterogeneous catalyst for acetalizing glycerol (a by-product formed during biodiesel synthesis) with acetone to produce solketal. Physicochemical characterization of the catalyst confirmed successful sulfonation. With 97.53% selectivity, the catalyst converted 94.89% glycerol into solketal under microwave heating conditions. The mesoporous nature, high acidity, and large surface area contribute to the high activity of the catalyst. The reaction is non-spontaneous and follows pseudo-first order kinetics with an E_a of 40.23 kJ mol^{-1}. A high glycerol conversion of 83.48%

was observed in the 5th catalytic cycle, showing the excellent stability of the catalyst upon repeated reuse without much loss of activity. Hence the preliminary results based on the lifecycle cost analysis and the mild reaction conditions, along with the catalyst reusability, indicate the potential suitability of the proposed method for achieving sustainable solketal production on an industrial scale.

Data availability

The datasets used and/or analyzed during the current study are available from the corresponding author on reasonable request.

Author contributions

Rhithuparna Devasan: conceptualization, investigation, methodology, writing – original draft; Shiva Prasad Gouda: writing – reviewing and editing; Gopinath Halder: supervision, project administration, writing – reviewing and editing; Samuel Lalthazuala Rokhum: conceptualization, methodology, supervision, project administration, writing – reviewing and editing.

Conflicts of interest

The authors confirm no conflict of interest.

Acknowledgements

The funding from the Department of Science and Technology, Science and Engineering Research Board (DST-SERB), Govt. of India vide project no. EEQ/2021/000167 is appreciatively acknowledged. We thank CIF NIT Silchar, IIT Indore, IIT Bombay, IIT Madras, IIT Kharagpur, and IIT Roorkee for the analysis.

References

1 I. Ambat, V. Srivastava and M. Sillanpää, *Renewable Sustainable Energy Rev.*, 2018, **90**, 356–369.
2 K. Saikia, K. Rajkumari, N. S. Moyon, S. Basumatary, G. Halder, U. Rashid and S. L. Rokhum, *Fuel Process. Technol.*, 2022, **238**, 107482.
3 Zulqarnain, M. Ayoub, M. H. M. Yusoff, M. H. Nazir, I. Zahid, M. Ameen, F. Sher, D. Floresyona and E. Budi Nursanto, *Sustain*, 2021, **13**, 1–28.
4 M. Tabatabaei, M. Aghbashlo, M. Dehhaghi, H. K. S. Panahi, A. Mollahosseini, M. Hosseini, M. M. Soufiyan, M. Tabatabaei, M. Aghbashlo and M. Dehhaghi, *et al.*, *Reactor technologies for biodiesel production and processing: a review*, 2019.
5 S. P. Gouda, J. M. H. Anal, P. Kumar, A. Dhakshinamoorthy, U. Rashid and S. L. Rokhum, *Catalysts*, 2022, **12**, 1312.
6 Y. K. Oh, K. R. Hwang, C. Kim, J. R. Kim and J. S. Lee, *Bioresour. Technol.*, 2018, **257**, 320–333.
7 J. V. L. Ruatpuia, B. Changmai, A. Pathak, L. A. Alghamdi, T. Kress, G. Halder, A. E. H. Wheatley and S. L. Rokhum, *Renew. Energy*, 2023, **206**, 597–608.
8 S. P. Gouda, A. Dhakshinamoorthy and S. L. Rokhum, *Chem. Eng. J. Adv.*, 2022, **12**, 100415.
9 M. H. Nazir, M. Ayoub, I. Zahid, R. B. Shamsuddin, S. Yusup, M. Ameen, Zulqarnain and M. U. Qadeer, *Biomass Bioenergy*, 2021, **146**, 105978.
10 S. Ao and S. L. Rokhum, *J. Chem.*, 2022, **2022**, 1–18.
11 L. Chen, B. Nohair, D. Zhao and S. Kaliaguine, *ChemCatChem*, 2018, **10**, 1918–1925.
12 Z. Yuan, S. Xia, P. Chen, Z. Hou and X. Zheng, *Energy Fuels*, 2011, **25**, 3186–3191.
13 R. Devasan, J. V. L. Ruatpuia, S. P. Gouda, P. Kodgire, S. Basumatary, G. Halder and S. L. Rokhum, *Sci. Rep.*, 2023, **13**, 1–17.
14 S. P. Gouda, K. Ngaosuwan, S. Assabumrungrat, M. Selvaraj, G. Halder and S. L. Rokhum, *Renewable Energy*, 2022, **197**, 161–169.
15 A. Das, D. Shi, G. Halder and S. Lalthazuala Rokhum, *Fuel*, 2022, **330**, 125511.
16 U. I. Nda-Umar, I. Ramli, Y. H. Taufiq-Yap and E. N. Muhamad, *Catalysts*, 2018, **9**, 15.
17 S. Sandesh, A. B. Halgeri and G. V. Shanbhag, *J. Mol. Catal. A: Chem.*, 2015, **401**, 73–80.
18 P. H. R. Silva, V. L. C. Gonçalves and C. J. A. Mota, *Bioresour. Technol.*, 2010, **101**, 6225–6229.
19 C. J. A. Mota, C. X. A. Da Silva, N. Rosenbach, J. Costa and F. Da Silva, *Energy Fuels*, 2010, **24**, 2733–2736.
20 A. R. Trifoi, P. S. Agachi and T. Pap, *Renewable Sustainable Energy Rev.*, 2016, **62**, 804–814.
21 M. R. Nanda, Y. Zhang, Z. Yuan, W. Qin, H. S. Ghaziaskar and C. Xu, *Renewable Sustainable Energy Rev.*, 2016, **56**, 1022–1031.
22 L. A. Bivona, A. Vivian, L. Fusaro, S. Fiorilli and C. Aprile, *Appl. Catal. B*, 2019, **247**, 182–190.
23 E. García, M. Laca, E. Pérez, A. Garrido and J. Peinado, *Energy Fuels*, 2008, **22**, 4274–4280.
24 I. Zahid, M. Ayoub, B. B. Abdullah, A. Mukhtar, S. Saqib, S. Rafiq, S. Ullah, A. G. Al-Sehemi, S. Farrukh and M. Danish, *ChemBioEng Rev.*, 2021, **8**, 227–238.
25 L. Aguado-Deblas, R. Estevez, M. Russo, V. La Parola, F. M. Bautista and M. L. Testa, *J. Environ. Chem. Eng.*, 2022, **10**, 108628.
26 E. G. R. T. Filho, E. L. Dall'Oglio, P. T. de Sousa, F. Ribeiro, M. Z. Marques, L. G. de Vasconcelos, M. P. N. de Amorim and C. A. Kuhnen, *Brazilian J. Chem. Eng.*, 2022, **39**, 691–703.
27 S. Ao, M. V. L. Chhandama, H. Li and S. L. Rokhum, *Curr. Microwave Chem.*, 2023, **10**, 3–25.
28 P. Priecel and J. A. Lopez-Sanchez, *ACS Sustainable Chem. Eng.*, 2019, **7**, 3–21.
29 S. M. Joshi, P. R. Gogate and S. Suresh Kumar, *Chem. Eng. Process. - Process Intensif.*, 2018, **124**, 186–198.
30 K. Rajkumari, B. Changmai, A. K. Meher, C. Vanlalveni, P. Sudarsanam, A. E. H. Wheatley and S. L. Rokhum, *Sustain. Energy Fuels*, 2021, **5**, 2362–2372.

31 C. N. Fan, C. H. Xu, C. Q. Liu, Z. Y. Huang, J. Y. Liu and Z. X. Ye, *React. Kinet., Mech. Catal.*, 2012, **107**, 189–202.
32 M. E. Davis, *Nature*, 2002, **417**, 813–821.
33 C. W. Jones, K. Tsuji and M. E. Davis, *Nature*, 1998, **393**, 52–54.
34 Y. Chu, H. Deng and J. Cheng, *J. Org. Chem.*, 2007, **72**, 7790–7793.
35 X. Li, Y. Jiang, R. Zhou and Z. Hou, *Appl. Clay Sci.*, 2019, **174**, 120–126.
36 X. Li, Y. Jiang, R. Zhou and Z. Hou, *Appl. Clay Sci.*, 2020, **189**, 105555.
37 X. Li, L. Zheng and Z. Hou, *Fuel*, 2018, **233**, 565–571.
38 G. S. Nair, E. Adrijanto, A. Alsalme, I. V. Kozhevnikov, D. J. Cooke, D. R. Brown and N. R. Shiju, *Catal. Sci. Technol.*, 2012, **2**, 1173–1179.
39 L. J. Konwar, A. Samikannu, P. Mäki-Arvela, D. Boström and J. P. Mikkola, *Appl. Catal., B*, 2018, **220**, 314–323.
40 M. Gonçalves, R. Rodrigues, T. S. Galhardo and W. A. Carvalho, *Fuel*, 2016, **181**, 46–54.
41 L. Wang, J. Zhang, S. Yang, Q. Sun, L. Zhu, Q. Wu, H. Zhang, X. Meng and F. S. Xiao, *J. Mater. Chem. A*, 2013, **1**, 9422–9426.
42 P. A. Oliveira, R. O. M. A. Souza and C. J. A. Mota, *J. Braz. Chem. Soc.*, 2016, **27**, 1832–1837.
43 Y. Jiang, R. Zhou, B. Ye and Z. Hou, *J. Ind. Eng. Chem.*, 2022, **110**, 357–366.
44 P. Manjunathan, S. P. Maradur, A. B. Halgeri and G. V. Shanbhag, *J. Mol. Catal. A: Chem.*, 2015, **396**, 47–54.
45 M. S. Rahaman, T. K. Phung, M. A. Hossain, E. Chowdhury, S. Tulaphol, S. B. Lalvani, M. O'Toole, G. A. Willing, J. B. Jasinski, M. Crocker and N. Sathitsuksanoh, *Appl. Catal., A*, 2020, **592**, 117369.
46 Fruit: world production by type 2021 | Statista, **https://www.statista.com/statistics/264001/worldwide-production-of-fruit-by-variety/**, (accessed 30 January 2023).
47 S. Ouyang, X. Kuang, Q. Xu and D. Yin, *J. Mater. Sci. Chem. Eng.*, 2014, **2**, 4–8.
48 K. Malins, J. Brinks, V. Kampars and I. Malina, *Appl. Catal., A*, 2016, **519**, 99–106.
49 B. Mallesham, P. Sudarsanam, G. Raju and B. M. Reddy, *Green Chem.*, 2013, **15**, 478–489.
50 I. B. Laskar, K. Rajkumari, R. Gupta and L. Rokhum, *Energy Fuels*, 2018, **32**, 12567–12576.
51 A. Mukherjee, B. Karmakar and G. Halder, *Chem. Eng. J. Adv.*, 2020, **1**, 100007.
52 M. S. Khayoon and B. H. Hameed, *Appl. Catal., A*, 2013, **464–465**, 191–199.
53 S. R. Churipard, P. Manjunathan, P. Chandra, G. V. Shanbhag, R. Ravishankar, P. V. C. Rao, G. Sri Ganesh, A. B. Halgeri and S. P. Maradur, *New J. Chem.*, 2017, **41**, 5745–5751.
54 Y. T. Wang, Z. Fang and F. Zhang, *Catal. Today*, 2019, **319**, 172–181.
55 L. Li, T. I. Korányi, B. F. Sels and P. P. Pescarmona, *Green Chem.*, 2012, **14**, 1611–1619.
56 J. M. Fraile, E. García-Bordejé and L. Roldán, *J. Catal.*, 2012, **289**, 73–79.
57 S. Ao, L. A. Alghamdi, T. Kress, M. Selvaraj, G. Halder, A. E. H. Wheatley and S. L. Rokhum, *Microwave-assisted valorization of glycerol to solketal using biomass-derived heterogeneous catalyst*, Elsevier, 2023, vol. 345.
58 A. H. Noor Armylisas, S. S. Hoong, T. I. Tuan Noor Maznee, S. K. Yeong and M. F. Mohammat, *J. Chem. Technol. Biotechnol.*, 2021, **96**, 2667–2674.
59 J. A. Vannucci, N. N. Nichio and F. Pompeo, *Catal. Today*, 2021, **372**, 238–245.
60 R. Zhou, Y. Jiang, H. Zhao, B. Ye, L. Wang and Z. Hou, *Fuel*, 2021, **291**, 1–9.
61 G. Vicente, J. A. Melero, G. Morales, M. Paniagua and E. Martín, *Green Chem.*, 2010, **12**, 899–907.
62 Y. Huang, G. Zhang and Q. Zhang, *ACS Omega*, 2021, **6**, 3875–3883.
63 R. Rodrigues, M. Gonçalves, D. Mandelli, P. P. Pescarmona and W. A. Carvalho, *Catal. Sci. Technol.*, 2014, **4**, 2293–2301.